Experimental Evaluations on 4-by-2 MU-MIMO Achieving 1 Gbps Throughput Using AMC with Outer-Loop Threshold Control for LTE-Advanced Downlink

Keisuke Saito†, Yuichi Kakishima†, Teruo Kawamura†, Yoshihisa Kishiyama†, Hidekazu Taoka‡, and Hidehiro Andoh†

†Radio Access Network Development Department,
NTT DOCOMO, INC.
3-5 Hikari-no-oka, Yokosuka-shi, Kanagawa-ken 239-8536 Japan

‡DOCOMO Communications Laboratories Europe GmbH
Landsberger Strasse 312, 80687, Munich, Germany

Abstract—**This paper presents laboratory experimental results on 4-by-2 multi-user (MU)-MIMO that achieves up to 1 Gbps throughput using carrier aggregation with a 100-MHz bandwidth in the LTE-Advanced downlink. The achievable throughput performance employing adaptive modulation and coding (AMC) with outer-loop threshold control based on acknowledgement (ACK) / negative ACK (NACK) feedback signaling in order to compensate for the fluctuation in the measured signal-to-interference plus noise ratio (SINR) value due to MU-MIMO multiplexing is evaluated using the implemented LTE-Advanced transceivers. Additionally, we evaluate the influence of the angle between spatially multiplexed users and the user combination in MU-MIMO operation with different received signal-to-noise ratio (SNR) conditions. Laboratory experimental results show that by performing AMC with outer-loop threshold control, the throughput of approximately 1 Gbps is achieved at the average received SNR of 30 dB. Furthermore, based on the experimental results, we confirm that angles narrower or wider than approximately 60 degrees between spatially multiplexed mobile stations (MSs) yield a lower ability to decrease the mutual interference using minimum mean square error (MMSE)-based precoding in 4-by-2 MU-MIMO. We also show that especially when the angle between spatially multiplexed MSs is narrower or wider than approximately 60 degrees, selecting the user pairs with a large difference in the average received SNR is effective in improving the total throughput.**

Keywords-LTE-Advanced; Multi-user MIMO; Adaptive modulation and coding; User pair selection; Experiment

I. INTRODUCTION

The 3rd Generation Partnership Project (3GPP) finalized the radio interface specifications for the next generation mobile communication system called Long-Term Evolution (LTE) as LTE Release 8 [1],[2]. LTE provides full IP packet-based radio access with low latency and adopts orthogonal frequency division multiple access (OFDMA) and single-carrier frequency division multiple access (SC-FDMA) as multiple access schemes in the downlink and uplink, respectively. In Japan, NTT DOCOMO launched a commercial LTE service in December 2010 under the new service brand of "Xi" (crossy) [3]. The 3GPP has put forth efforts towards standardizing the enhanced LTE radio interface called LTE-Advanced (LTE Release 10 and beyond) and specifications for LTE Release 10 were finalized [4],[5]. In LTE-Advanced, it is necessary to support a wider bandwidth than that in LTE Release 8, i.e., 20 MHz, to satisfy the high level requirements corresponding to the target peak data rate of greater than 1 Gbps. Toward this end, LTE-Advanced supports carrier aggregation (CA) up to 100 MHz by aggregating multiple component carriers (CCs) with backward compatibility to LTE Release 8. In addition, to satisfy the requirements for further improvement in spectrum efficiency, enhanced multiple-input multiple-output (MIMO) techniques such as higher-order MIMO multiplexing and multi-user (MU)-MIMO are supported.

In [6], we reported laboratory experimental results that show that the total downlink throughput performance of 1 Gbps can be achieved by applying 4-by-2 MU-MIMO with 2 mobile stations (MSs) and CA with 5 CCs (100-MHz bandwidth) based on experimental equipment employing the LTE-Advanced radio interface with a demodulation reference signal (DM-RS) and channel state information (CSI) reference signal (CSI-RS). In order to achieve the total throughput of 1 Gbps, spatial multiplexing with the total of four data streams is necessary when applying 4-by-2 MU-MIMO multiplexing using a 100-MHz bandwidth. However, when the base station (BS) spatially multiplexes the maximum of four data streams, which exceeds the number of receiver antennas per MS, very accurate CSI feedback is required so that the BS can generate precoding weights to decrease the mutual interference between transmitted data streams of spatially multiplexed MSs [7]-[9]. Therefore, in our experimental equipment, extended CSI feedback based on eigenvalue decomposition (EVD) is implemented to evaluate the potential performance of LTE-Advanced MU-MIMO although it is not yet standardized as an LTE-Advanced specification.

In this paper, we present further laboratory experimental results on 4-by-2 MU-MIMO with two MSs that achieves up to 1 Gbps throughput using CA with a 100-MHz bandwidth in the LTE-Advanced downlink. Compared to [6], this paper further evaluates the effect when applying adaptive modulation and coding (AMC) to 4-by-2 MU-MIMO operation. In order to compensate for the fluctuation in the measured signal-to-interference plus noise ratio (SINR) value due to MU-MIMO multiplexing, outer-loop threshold control based on acknowledgement (ACK) / negative ACK (NACK) feedback signaling is applied to the modulation and coding scheme (MCS) selection for AMC. Additionally, we evaluate the influence of the angle between spatially multiplexed users and the user combination with different received signal-to-noise ratio (SNR) conditions. The rest of the paper is organized as follows. In Section II, the MU-MIMO scheme implemented for experimental evaluation is outlined. After the configuration of the implemented transceiver is described in Section III, the laboratory experimental results are presented in Section IV. Finally, Section V presents our conclusions.

II. MU-MIMO SCHEME FOR EXPERIMENTAL EVALUATIONS

A. Time/Frequency Granularity for MU-MIMO Operation

In the paper, downlink MU-MIMO with a single BS and two MSs is evaluated in laboratory experiments, where the number of BS transmitter antennas, N_{TX}, is four and the number of receiver antennas for each MS, N_{RX}, is two. In the frequency domain, each CC consists of multiple subbands (SBs), where a SB corresponds to a unit of the CSI feedback from the MSs. Each SB has the

978-1-4673-0990-5/12/$31.00 ©2012 IEEE

bandwidth of F_{CSI} and consists of multiple resource blocks (RBs), each of which contains 12 subcarriers. In the time domain, the reference signal (RS) used for CSI estimation, i.e., the CSI-RS, for each transmitter antenna is periodically multiplexed with the time duration of T_{CSI} and mapped every 6 subcarriers in the frequency domain (note that multiplexing for every 12 subcarriers is supported in the LTE Release 10 specification [10]), where frequency domain multiplexing (FDM) is used to multiplex CSI-RSs between transmitter antennas. Thus, the precoding weights for MU-MIMO operation are updated with the same periodicity as that for the CSI-RS with the additional control delay of 10 msec. The RS used for demodulation of each data stream, i.e., DM-RS, which is precoded in the same manner as the data streams, is multiplexed with the insertion density of 12 resource elements (REs) per RB and within each subframe. In MU-MIMO with two streams per MS, code division multiplexing (CDM) is used to multiplex the DM-RSs between two data streams within the same MS, and FDM is used between two MSs. In MU-MIMO with one stream per MS, CDM is applied to multiplex the DM-RSs between two MSs.

B. CSI Feedback Scheme

The MS calculates the CSI as feedback information and transmits it to the BS. In the paper, the MS calculates the eigenvectors and the eigenvalues of the covariance matrix of the measured channel, and the received SINR of each SB. At the u-th MS (u = 1 or 2), the downlink channel matrix ($N_{RX} \times N_{TX}$) on the k-th subcarrier, $\mathbf{H}_u(k)$, is estimated using the received CSI-RS, which is denoted as $\hat{\mathbf{H}}_u(k)$. Then, the covariance matrix for each SB, $\overline{\mathbf{R}}_u$, is calculated by averaging $\hat{\mathbf{H}}_u^{\mathrm{H}}(k)\hat{\mathbf{H}}_u(k)/S_u$ within the SB in the frequency domain, where S_u is the average received CSI-RS power for the normalization to remove the effect of path loss and shadowing. Below, the calculation of CSI feedback within a SB is presented and the index of the SB is omitted for simplicity. By applying the Jacobi EVD [11] to the channel covariance matrix as $\overline{\mathbf{R}}_u = \mathbf{U}_u\mathbf{D}_u^2\mathbf{U}_u^{\mathrm{H}}$, the eigenvalues $\mathbf{D}_u^2 = \mathrm{diag}\{\lambda_{u,1}^2\ \lambda_{u,2}^2\ \lambda_{u,3}^2\ \lambda_{u,4}^2\}$ for $\lambda_{u,1}^2 \ge \lambda_{u,2}^2 \ge \lambda_{u,3}^2 \ge \lambda_{u,4}^2$, and the corresponding eigenvectors, $\mathbf{U}_u = (\mathbf{u}_{u,1}\ \mathbf{u}_{u,2}\ \mathbf{u}_{u,3}\ \mathbf{u}_{u,4})$, are derived. The two highest eigenvalues and the corresponding eigenvectors are selected for the CSI feedback since the spatial multiplexing of the maximum of two data streams per MS is assumed. Furthermore, the SINR for the i-th data stream (i = 1 or 2) of the u-th MS is calculated by $\gamma_{u,i} = \lambda_{u,i}^2 S_u/\sigma_u^2$, where σ_u^2 is the average noise power estimated using the received CSI-RS. Each complex eigenvector component is quantized by 13 bits using star-type mapping (7 bits for phase and 6 bits for amplitude) for each transmitter antenna, and the eigenvalue and SINR for each data stream are quantized by 5 and 7 bits, respectively. The MS feeds back the control signals to the BS via the uplink shared channel.

C. Precoding Weight Generation Scheme

At the BS transmitter, the precoding weights for downlink MU-MIMO are calculated based on the CSI transmitted from the two MSs in the uplink. Here, the composite channel matrix for each SB of the u-th MS is defined as $\mathbf{G}_u = (\hat{\lambda}_{u,1}\hat{\mathbf{u}}_{u,1}\ \ \hat{\lambda}_{u,2}\hat{\mathbf{u}}_{u,2})^{\mathrm{H}}$, where $\hat{\lambda}_{u,i}$ and $\hat{\mathbf{u}}_{u,i}$ are the quantized eigenvalue and the corresponding eigenvector, respectively. The precoding weight matrix for each SB, $\mathbf{V}$, is defined as $\mathbf{V} = (\mathbf{v}_{1,1}\ \mathbf{v}_{1,2}\ \mathbf{v}_{2,1}\ \mathbf{v}_{2,2})$, where $\mathbf{v}_{u,i}$ is the $N_{TX} \times 1$ precoding weight vector. Matrix $\mathbf{V}$ is calculated based on the minimum mean square error (MMSE) criteria as

$$\mathbf{V} = \mathbf{G}^{\mathrm{H}}(\mathbf{G}\mathbf{G}^{\mathrm{H}} + \mathbf{E})^{-1}, \tag{1}$$

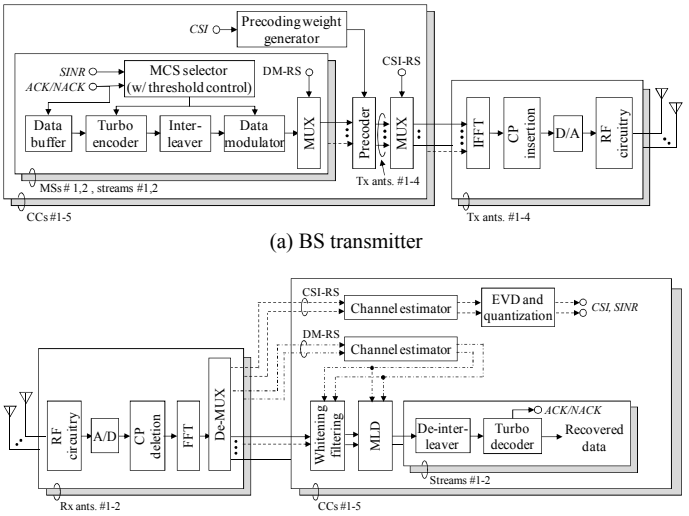

Figure 1. Configuration of implemented LTE-Advanced transceiver.

where $\mathbf{G} = \left(\mathbf{G}_1^{\mathrm{T}}\ \mathbf{G}_2^{\mathrm{T}}\right)^{\mathrm{T}}$, $\mathbf{E} = \mathrm{diag}\{\hat{\gamma}_{1,1}^{-1}\ \hat{\gamma}_{1,2}^{-1}\ \hat{\gamma}_{2,1}^{-1}\ \hat{\gamma}_{2,2}^{-1}\}$, and $\hat{\gamma}_{u,i}$ is the quantized SINR reported by the MSs. By using the normalized precoding weights, $\overline{\mathbf{v}}_{u,i} = \mathbf{v}_{u,i}/\|\mathbf{v}_{u,i}\|$, the transmission signal vector (N_{TX} = 4) on the k-th subcarrier is represented as

$$\mathbf{s}(k) = \sum_{u=1}^{2}\sum_{i=1}^{2}\overline{\mathbf{v}}_{u,i}d_{u,i}(k), \tag{2}$$

where $d_{u,i}(k)$ represents the modulated data sequence. Furthermore, $\overline{\mathbf{v}}_{u,i}$ is constant within the SB but varies among the SBs although the index of the SB has been omitted for simplicity.

III. Configuration of Implemented LTE-Advanced Transceiver

A. Implemented OFDMA Transmitter and Receiver

The configuration of the implemented LTE-Advanced transmitter and receiver and the major radio link parameters are given in Fig. 1 and Table I, respectively. The transmission bandwidth and the number of subcarriers of the OFDMA signal in the downlink are 90 MHz and 6000, respectively (thus, the subcarrier separation is 15 kHz). We employ CA using 5 CCs (each CC has an 18-MHz transmission bandwidth, which is supported in LTE Release 8) with contiguous spectrum allocation. We assume a 4-by-2 MU-MIMO antenna configuration with the number of MSs of two. In the paper, F_{CSI} and T_{CSI} for MU-MIMO operation are set to 900 kHz (= 5 RBs) and 5 msec, respectively. In the BS transmitter, the information binary data sequence for each data stream and CC is independently turbo encoded with the coding rate of R and modulated by QPSK, 16QAM, or 64QAM. After multiplying the precoding weights for MU-MIMO, the modulated data sequence for each transmitter antenna is converted into an OFDM symbol with the duration of 66.67 μsec using an 8192-point inverse FFT (IFFT) followed by the addition of a cyclic prefix (CP) of 4.69 μsec. After conversion into baseband in-phase (I) and quadrature (Q) components using digital-to-analog converters, quadrature modulation is performed. Finally, the intermediate frequency (IF) modulated signal is up-converted into a radio frequency (RF) signal and amplified by the power amplifier, where the center carrier frequency is 3.92625 GHz.

At each MS receiver, we apply two-branch antenna diversity reception. The frequency down-converted IF signal is first linearly amplified by an automatic gain control (AGC) amplifier with the

TABLE I. MAJOR RADIO LINK PARAMETERS

OFDM signal bandwidth		90 MHz (18 MHz × 5 CCs)
Number of subcarriers		6000 (1200 × 5 CCs)
Subcarrier separation		15 kHz
Subframe length		1 msec (14 OFDM symbols)
OFDM symbol duration	Effective data	66.67 μsec
	Cyclic prefix	4.69 μsec
Number of BS transmitter antennas		4
Number of MS receiver antennas		2
Number of MSs		2
Channel coding / decoding		Turbo coding / Max-Log-MAP decoding (6 iterations)
Channel model		6-path exponentially-decayed Rayleigh fading model
Control delay for precoding		10 msec
Control delay for AMC		8 msec
HARQ	Packet combining	Incremental redundancy (IR)
	Max. number of transmissions	3
	Round trip delay	8 msec

dynamic range of approximately 50 dB. The received signal is converted into baseband I and Q components by a quadrature detector. The I and Q signals are converted into a digital format using 14-bit analog-to-digital converters. After the CP is removed, the OFDMA signal is de-multiplexed into each subcarrier component using an 8192-point FFT. Channel estimation for MIMO signal detection is performed for each SB using the DM-RS. The signal detection scheme based on the maximum likelihood detection (MLD) is applied to separate the two data streams that are transmitted to its own MS. Furthermore, an interference whitening filter is applied before the MLD operation in order to randomize the interfering data streams that are transmitted to the other MS [12],[13]. Finally, the sequence of likelihood values after MLD is turbo decoded using the Max-Log-MAP algorithm with six iterations to recover the transmitted binary data.

Table II summarizes the set of nine MCSs used for AMC in the experiments. The AMC is performed according to the instantaneous received SINR reported by the MS. In order to compensate for the fluctuation in the reported SINR values, the threshold for MCS selection is adaptively adjusted by using outer-loop control based on ACK/NACK feedback signaling from the MS [14] as shown in Fig. 2. When ACK signaling is received at the BS, the threshold for MCS selection is decreased by $\Delta_{step}T_{BLER}$; otherwise, i.e., NACK signaling is received, the threshold is increased by $\Delta_{step}(1-T_{BLER})$, where Δ_{step} and T_{BLER} indicate the step size of threshold adjustment and target block error rate (BLER), respectively. In the paper, Δ_{step} and T_{BLER} are set to 0.1 dB and 10%, respectively, and we assume that the threshold for all MCSs is commonly adjusted by applying the outer-loop threshold control. The control delay of AMC is 8 msec. We use incremental redundancy for hybrid automatic repeat request (HARQ) with packet combining and the round trip delay is 8 msec.

B. Configuration of Laboratory Experiment

The configuration for the laboratory experimental system using the multi-path fading simulators is shown in Fig. 3. The fading simulators generate a 6-path exponentially-decayed power delay profile with the root mean squared (r.m.s.) delay spread value of 0.3 μsec, where the relative path power is decayed by 2 dB and each path is independently Rayleigh-faded with the maximum Doppler frequency of 10 Hz corresponding to the moving speed of approximately 3 km/h at the carrier frequency of 3.92625 GHz. Then, additive white Gaussian noise (AWGN) is added at the input of each receiver antenna for each MS. In the experiments, we assume highly-correlated transmitter antenna pairs. The fading correlation between the highly-correlated transmitter antennas is set to 0.99 and that between antenna pairs is set to zero assuming indoor or field environments with a relatively small multipath angular spread. Meanwhile, the fading correlation between receiver antennas is set to zero.

TABLE II. MCS SET FOR AMC

Index	Modulation	Coding rate	Index	Modulation	Coding rate
1	QPSK	0.39	6	64QAM	0.47
2		0.47	7		0.56
3	16QAM	0.38	8		0.65
4		0.49	9		0.73
5		0.58			

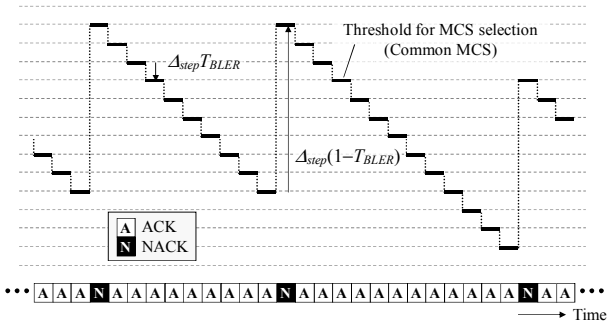

Figure 2. Operation principle of outer-loop threshold control.

IV. LABORATORY EXPERIMENTAL RESULTS

A. Throughput Performance Using AMC with Outer-Loop Threshold Control

Figure 4 shows the throughput performance employing AMC and HARQ for MU-MIMO with 2 data streams per MS, which is defined as the aggregated throughput for each MS, as a function of the average received SNR per receiver antenna. In the evaluation, the same average received SNR is assumed for the two MSs. The direction of departure (DoD) for the u-th MS, DoD_u, is set to $\{\mathrm{DoD}_1 / \mathrm{DoD}_2\} = \{+30 / -30\}$ degrees. The throughput performance for the respective MCS sets is also given for comparison, and in this case the same MCS combination is assumed for the two MSs. Moreover, we utilize the higher MCS for the first stream compared to that for the second stream because the eigenvalue of the first stream is higher than that for the second stream as described in Section II-*B*. Figure 4 shows that by employing MCS combinations $\{\mathrm{MCS}_1 / \mathrm{MCS}_2\}$ = {64QAM, R = 0.73 / 64QAM, R = 0.56}, where MCS_i denotes the MCS for the i-th data stream, the throughput of approximately 1 Gbps is achieved at the average received SNR of 30 dB. Furthermore, we clearly find that by applying AMC with outer-loop threshold control, nearly the maximum throughput at each average received SNR is achieved, since the appropriate MCS is selected based on the instantaneous measured SINR. As a result, we observe that the throughput values of 500 Mbps and 1 Gbps are

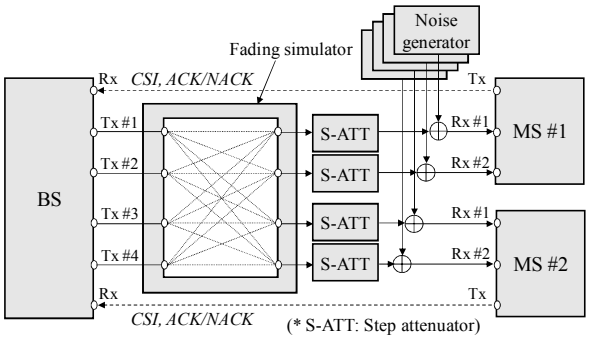

Figure 3. Configuration of laboratory experimental system.

achieved at the average received SNR of approximately 15 and 30 dB, respectively.

Figures 5(a) and 5(b) show the throughput performance comparison between MU-MIMO and single-user (SU)-MIMO as a function of the average received SNR per receiver antenna when $\{DoD_1 / DoD_2\} = \{+30 / -30\}$ and $\{+15 / -15\}$ degrees, respectively. In each figure, we plot the throughput employing AMC and HARQ for MU-MIMO and SU-MIMO with one and two data streams per MS. In MU-MIMO, the same average received SNR is assumed for the two MSs. Moreover, we employ SU-MIMO with precoding based on CSI feedback, which is identical to that for MU-MIMO. Figure 5(a) shows that when $\{DoD_1 / DoD_2\} = \{+30 / -30\}$ degrees, the peak throughput of approximately 570 Mbps is achieved at the average received SNR of 26 dB for SU-MIMO. Furthermore, assuming rank adaptation, i.e., semi-statically switching the number of data streams per MS according to the channel conditions, the required average received SNR to achieve the throughput of 500 Mbps for MU-MIMO is significantly reduced by approximately 7 dB compared to that for SU-MIMO. When $\{DoD_1 / DoD_2\} = \{+15 / -15\}$ degrees, improvement in the required average received SNR compared to that for SU-MIMO becomes smaller by approximately 4 dB due to the increase in the mutual interference between transmitted data streams of spatially multiplexed MSs as shown in Fig. 5(b).

Figure 6 shows the throughput performance employing AMC and HARQ for MU-MIMO as a function of the DoD. In the figure, we plot the throughput for MU-MIMO with two and one stream per MS at the average received SNR of 24.1 and 12.1 dB, respectively. The same average received SNR is assumed for the two MSs. Figure 6 shows that the highest throughput is achieved when $\{DoD_1 / DoD_2\} = \{+30 / -30\}$ degrees since the amount of mutual interference between spatially multiplexed MSs is minimized. This figure also shows that the impact of the mutual interference on the achievable throughput for two streams per MS is greater than that for one stream per MS. These results indicate that user pair selection in the spatial domain is essential to maximizing the achievable throughput for MU-MIMO.

B. Influence of User Combination with Different Received SNRs in MU-MIMO

Figure 7 shows the user throughput performance for MU-MIMO with two streams per MS considering the user combination with different average received SNR conditions. AMC and HARQ are applied in the evaluation. The horizontal and vertical axes represent the average received SNR for MS #1 and MS #2, respectively, and the colors indicate the throughput values for MS #1. Figure 7(a) shows that when $\{DoD_1 / DoD_2\} = \{+30 / -30\}$ degrees, almost the same throughput performance is achieved under the identical average received SNR conditions irrespective of the average received SNR values for MS #2. When $\{DoD_1 / DoD_2\} = \{+15 / -15\}$ degrees, the achievable throughput is decreased according to the increase in the average received SNR values for MS #2 as shown in Fig. 7(b). This is because the ability to suppress the mutual interference using MMSE-based precoding in 4-by-2 MU-MIMO in the case of $\{DoD_1 / DoD_2\} = \{+15 / -15\}$ degrees is less than that in the case of $\{DoD_1 / DoD_2\} = \{+30 / -30\}$ degrees as shown in Fig. 6.

Finally, Fig. 8 shows the total throughput performance, which is defined as the aggregated throughput for each MS, considering the user combination with different average received SNR conditions. The evaluation conditions are identical to those in Fig. 7. The figure shows that especially when the average received SNR conditions between spatially multiplexed MSs are almost the same in the case of $\{DoD_1 / DoD_2\} = \{+15 / -15\}$ degrees, the achievable throughput is widely degraded compared to that in the case of

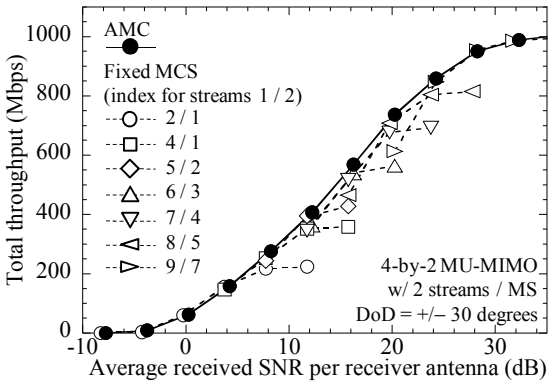

Figure 4. Throughput performance of MU-MIMO using AMC with outer-loop threshold control.

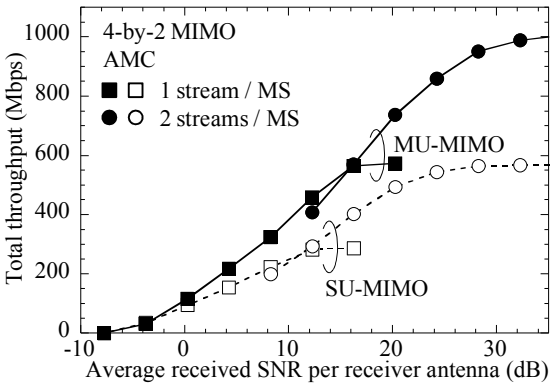

(a) DoD = +/– 30 degrees

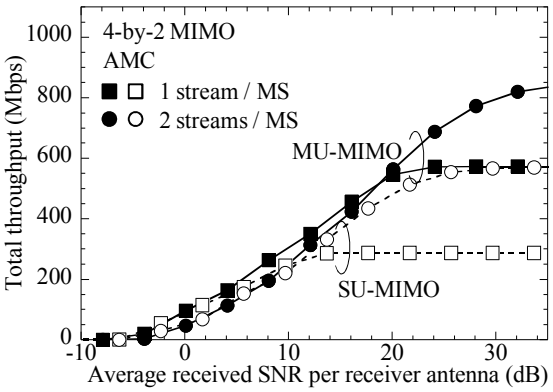

(b) DoD = +/– 15 degrees

Figure 5. Throughput performance comparison between MU-MIMO and SU-MIMO.

$\{DoD_1 / DoD_2\} = \{+30 / -30\}$ degrees. Meanwhile, when the difference in the received SNR between MSs is large, the degradation of achievable throughput is relatively small. It should be noted that in the region the achievement of greater throughput is expected by applying rank adaptation, although the performance for MU-MIMO with two streams per MS is shown in Fig. 8. Therefore we discuss the MU-MIMO throughput performance when rank adaptation is applied, which means that the number of data streams per MS is semi-statically switched according to the average received SNR. For example, we consider 4 user combinations, $\{SNR_1, SNR_2\} = \{0, 0\}$, $\{20, 20\}$, $\{0, 20\}$ and $\{20, 0\}$ dB, where SNR_u denotes the average received SNR for the u-th MS and which correspond to rank-2, rank-4, and rank-3 transmission, respectively.

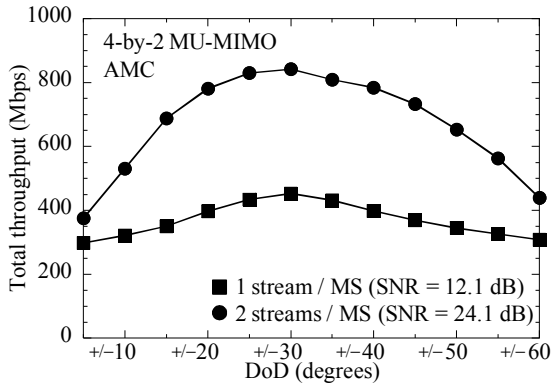

Figure 6. Total throughput considering MS combination with different DoDs.

In this case, the achievable throughput values for the respective user combinations are summarized in Table III. When round-robin scheduling is performed between user combinations {SNR_1, SNR_2} = {0, 0} and {20, 20} dB, the total average throughput becomes approximately 426 and 330 Mbps for {DoD_1 / DoD_2} = {+30 / −30} and {+15 / −15} degrees, respectively. When the round-robin scheduling is performed between the user combinations {SNR_1, SNR_2} = {0, 20} and {20, 0} dB, the total average throughput becomes approximately 438 and 396 Mbps, respectively. As a result, the latter increases the total throughput by approximately 20% compared to the former in the case of {DoD_1 / DoD_2} = {+15 / −15} degrees. Therefore, we clearly find that when the angle between spatially multiplexed MSs is narrower (or wider) than approximately 60 degrees such as {DoD_1 / DoD_2} = {+30 / −30}, selecting the user pairs with a large difference in the average received SNR conditions is effective in improving the total throughput.

V. Conclusion

This paper presented laboratory experimental results on 4-by-2 MU-MIMO that achieves up to 1 Gbps throughput using CA with a 100-MHz bandwidth in the LTE-Advanced downlink. The achievable throughput performance employing AMC with outer-loop threshold control based ACK/NACK feedback signaling in order to compensate for the fluctuation in the measured SINR value due to MU-MIMO multiplexing was evaluated using the implemented LTE-Advanced transceivers. Additionally, we evaluated the influence of the angle between spatially multiplexed users and the user combination in MU-MIMO operation under different received SNR conditions. Laboratory experimental results showed that by performing AMC with outer-loop threshold control, the throughput of approximately 1 Gbps is achieved at the average received SNR of 30 dB. Furthermore, we confirmed that when the angle between spatially multiplexed MSs is narrower or wider than approximately 60 degrees yield a lower ability to decrease the mutual interference using MMSE-based precoding in 4-by-2 MU-MIMO operation. We also showed that when the angle between spatially multiplexed MSs is narrower or wider than approximately 60 degrees, selecting the user pairs with a large difference in the average received SNR is effective in improving the total throughput. Based on the experimental results, we clarified that the user pairing for MU-MIMO operation should be performed considering the angle between spatially multiplexed users and the received SNR for each user in order to maximize the achievable throughput.

References

[1] 3GPP, TS 36.300 (V8.12.0), "Evolved Universal Terrestrial Radio Access (E-UTRA) and Evolved Universal Terrestrial Radio Access Network (E-UTRAN); Overall description," Apr. 2010.

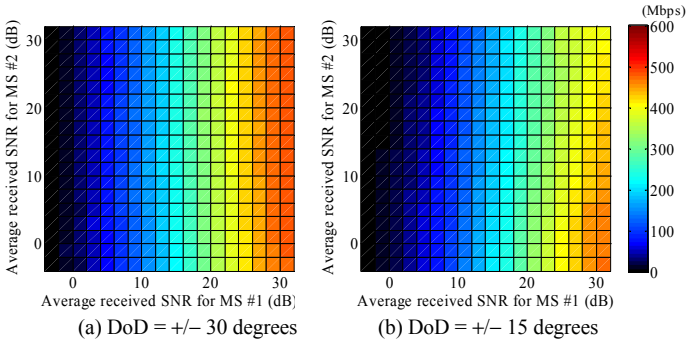

(a) DoD = +/− 30 degrees (b) DoD = +/− 15 degrees

Figure 7. User throughput considering MS combination with different SNRs.

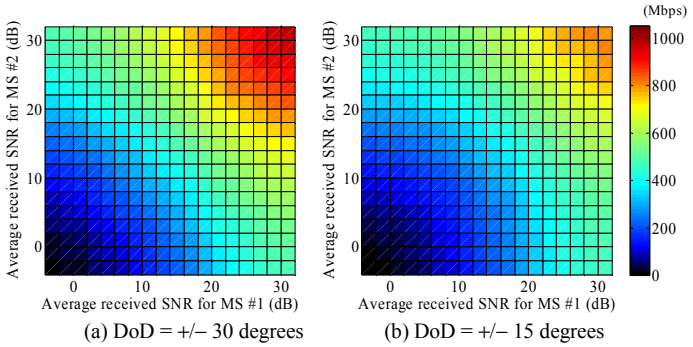

(a) DoD = +/− 30 degrees (b) DoD = +/− 15 degrees

Figure 8. Total throughput considering MS combination with different SNRs.

TABLE III. Example of Total Throughput for Respective User Combination

User combination {SNR_1, SNR_2}	DoD = +/−30 degrees	DoD = +/−15 degrees
{0, 0} dB	115.0 Mbps	96.3 Mbps
{20, 20} dB	736.8 Mbps	563.3 Mbps
{0, 20} dB	437.6 Mbps	395.6 Mbps
{20, 0} dB	437.6 Mbps	395.6 Mbps

[2] M. Tanno, Y. Kishiyama, N. Miki, K. Higuchi, and M. Sawahashi, "Evolved UTRA - physical layer overview," *Proc. IEEE SPAWC 2007*, June 2007.
[3] http://www.nttdocomo.com/pr/2010/001494.html
[4] 3GPP, TS 36.201 (V10.0.0), "Evolved Universal Terrestrial Radio Access (E-UTRA); LTE physical layer; General description (Release 10)," Dec. 2010.
[5] E. Dahlman, S. Parkvall, and J. Sköld, 4G –LTE/LTE-Advanced for Mobile Broadband, Academic press, 2011.
[6] Y. Kakishima, T. Kawamura, Y. Kishiyama, H. Taoka, and T. Nakamura, "Experimental evaluations on carrier aggregation and multi-user MIMO associated with EVD-based CSI feedback for LTE-Advanced downlink," *Proc. IEEE ISWCS'11*, Nov. 2011.
[7] D. Love, R. Heath, V. Lau, D. Gesbert, B. Rao, and M. Andrews, "An overview of limited feedback in wireless communication systems," IEEE J. Sel. Areas Commun., vol. 26, no. 8, pp. 1341-1365, Oct. 2008.
[8] M. Trivellato, F. Boccardi, and H. Huang, "On transceiver design and channel quantization for downlink multiuser MIMO systems with limited feedback," IEEE J. Sel. Areas Commun., vol. 26, no. 8, pp. 1494-1504, Oct. 2008.
[9] C. Guthy, W. Utschick, and G. Dietl, "Finite rate feedback schemes for the MIMO OFDM broadcast channel," International ITG Workshop on Smart Antennas - WSA 2008, Feb. 2008.
[10] 3GPP, TS 36.211 (V10.3.0), "Evolved Universal Terrestrial Radio Access (E-UTRA); Physical channels and modulation," Sep. 2011.
[11] B. T. Smith, J. M. Boyle, and J. J. Dongarra, Matrix Eigensystem Routines – EISPACK Guide, 2nd ed., vol. 6 of lecture notes in computer science, Springer, 1988.
[12] D. Tue and P. Viswanath, Fundamentals of wireless communication, 2008.
[13] S. Shim, "Block diagonalization for multi-user MIMO with other-cell interference," IEEE Trans. on Wireless Commun.
[14] J. Lee, R. Arnott, K. Hamabe, and N. Takano, "Adaptive modulation switching level control in high speed downlink packet access transmission," 3G Mobile Communication Technologies, pp. 156-159, May 2002.